IET Microwaves, Antennas & Propagation

Research Article

IET Journals
The Institution of Engineering and Technology

Efficient computation of the reduced matrix of MLFMA–CBFM for electrically large blocks

ISSN 1751-8725
Received on 8th October 2019
Revised 13th January 2020
Accepted on 11th February 2020
E-First on 19th March 2020
doi: 10.1049/iet-map.2019.0814
www.ietdl.org

Eliseo García[1] ✉, Lorena Lozano[2], Carlos Delgado[2], Felipe Cátedra[2]

[1]*Automatics Department, University of Alcalá, Alcalá de Henares, Spain*
[2]*Computer Science Department, University of Alcalá, Alcalá de Henares, Spain*
✉ *E-mail: eliseo.garcia@uah.es*

Abstract: In recent years, the characteristic basis function method has been developed as an efficient approach for the solution of large electromagnetic radiation or scattering problems. According to this technique, the currents over the scenario under analysis are defined using a set of pre-computed characteristic basis functions, associated with a number of blocks into which the geometry is partitioned. This involves some computational advantages due to the reduction of the number of unknowns compared to conventional approaches. However, additional pre-processing time is introduced due to the computation of the CBFs and the reduced coupling matrix. A novel strategy is presented in this study in order to accelerate the generation of the reduced matrix, based on the application of the multilevel fast multipole algorithm.

1 Introduction

There is a growing interest in the analysis of electrically large objects applying rigorous techniques at the present time, substituting in some cases conventional asymptotic approaches such as the geometrical theory of diffraction (GTD) [1], physical optics (PO) [2] or their combination [3–6]. Due to the size of the problems, high-frequency methods were, in past years the only option for the analysis of medium or large problems due to their relaxed computational requirements. However, the application range of full-wave analysis methods has been greatly extended due to the parallelisation of electromagnetic algorithms, the new capabilities of modern hardware architectures and the development of novel efficient numerical techniques.

The method of moments (MoM) [7] has been extensively applied to the electromagnetic analysis of geometries with arbitrary shapes defined by perfectly electric conductor (PEC) surfaces or containing thin layers of dielectric material. It is a reference for the development of new approaches in order to address problems related to scattering or radiation involving arbitrary 3D geometries. The MoM generates a system of linear equations whose solution represents the values of the current associated with each one of the basis functions. The geometry needs to be discretised into subpatches with a size typically around $\lambda/10$ to obtain accurate results.

The main restriction of the MoM is the size of its matrix when the electrical size of the scenario increases, and this is caused because of the quadratic relationship between the number of the subpatches in the discretisation process and the frequency of the problem, producing computationally large problems even for moderately sized geometries, which leads to restrictive CPU time and memory requirements.

Several techniques have appeared in order to overcome this issue, whose goal is to render full-wave simulations affordable for larger geometries. One group of these approaches, which have become very popular in recent years, is the fast multipole method [8] (FMM) and, its multilevel version, the multi-level fast multipole algorithm (MLFMA) [9]. The computational complexity, in this case, is decreased from $O(N2)$ to $O(N3/2)$ and to $O(N\log N)$, respectively, because the matrix–vector products are computed efficiently in the solution process, and only the near-field terms of the coupling matrix are required to be stored.

There are numerical approaches that benefit from an improvement of the efficiency using strategies based on the reduction of the number of unknowns. These techniques divide the geometry into blocks or domains, and define a group of macro-basis functions on each of the blocks. The synthetic function expansion (SFX) technique [10], as well as the characteristic basis function method [11–14] (CBFM), are examples of approaches based on this strategy.

The CBFM represents the current on the surface of the objects using high-level basis functions rather than the subdomain-type functions related to the traditional MoM (rooftops, Rao–Wilton–Glisson functions, etc.). The high-level basis functions are called characteristic basis functions (CBFs) defined on the blocks as aggregations of low-level functions. The main goal of the CBFM is the reduction of the total number of unknowns considering the physics of the problem and the geometrical properties of the objects. This reduction, in turn, decreases the size of the coupling matrix, known as a reduced matrix in the CBFM and, as a consequence, direct solvers can be applied for moderately sized problems. However, iterative solvers are still required for the solution of electrically large problems, since the size of the reduced matrix can preclude using direct solvers in this case. The generalised minimal residue method [15] (GMRES) and the bi-conjugated stabilised gradient method [16] (BiCGStab) are iterative solvers with the proved performance that have been applied in the present work.

Some efficient approaches have been recently developed to relax the computational requirements of the CBFM when analysing electrically large or very large objects. The authors described in [17] a technique to increase the efficiency of the iterative solution process for radar cross-section (RCS) applications, based on the elimination of unknowns associated with non-significant contributions. The CBFM is combined with the adaptive cross approximation approach in [18], based on the compression of rank-deficient coupling submatrices containing interactions between distant functions. A study of the efficiency resulting from applying different block sizes is presented in [19]. A fast algorithm for the generation of macro basis functions exploiting the geometrical redundancy of antenna arrays is explained in [20]. An approach for the direct solution of scattering problems using the CBFM can be seen in [21].

The CBFM and MLFMA can be combined in order to obtain improved efficiency [22], replacing the subdomain basis functions by CBFs and considering the computation and storage of only the functions related to surrounding blocks. The rest of the interactions is accounted for in the iterative solution process, improving the

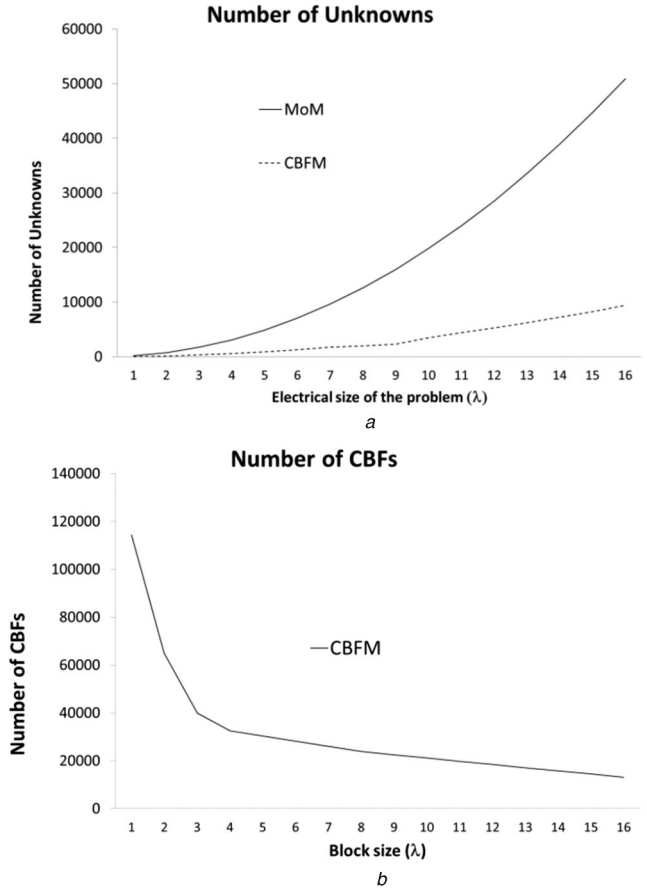

Fig. 1 *Comparison of the number of unknowns*
(a) Between the MoM and the CBFM, ***(b)*** Applying the CBFM with different block sizes

memory requirements and CPU time with respect to MoM or MoM-MLFMA. In this work, we present a more efficient procedure for the computation of these terms.

Due to the rapid increase in the performance of modern multi-core computing systems, the parallelisation of existing numerical techniques has been widely adopted [23–25], which makes scalability a fundamental factor when developing new simulation algorithms. The examples shown in this work make use of a parallel implementation of the presented algorithm in order to address realistic scenarios.

The remaining part of this paper is organised as follows: we present a review of the MoM and a description of the MLFMA in Section 2, pointing out their main advantages. In Section 3, the CBFM is introduced, and its combination with the MLFMA is described in Section 4. Next, the proposed technique is outlined in Section 5. Experimental results are shown in Section 6 and, finally, Section 7 contains the main conclusions derived from this work.

2 Description of MLFMA–MoM

The MoM [7] transforms the integro-differential equations that define the physics of the problem into linear equation (1). It requires the discretisation of the geometry and the definition of a set of basis and testing functions to represent the unknowns imposing the appropriate boundary conditions. The MoM requires the computation of the coupling matrix $[\boldsymbol{Z}]$, the impressed voltage vector $[\boldsymbol{V}]$ associated to the external excitations and the induced current vector $[\boldsymbol{J}]$ containing the coefficients to be determined:

$$[\boldsymbol{V}] = [\boldsymbol{Z}][\boldsymbol{J}] \tag{1}$$

The conventional MoM requires the solution of (1) using the full coupling matrix $[\boldsymbol{Z}]$. For electrically moderate or large scenarios, however, the direct solution of this system can consume a considerable amount of CPU-time and memory. Some techniques, such as the multilevel fast multipole algorithm, compensate this limitation by storing only the coupling matrix terms that involve interactions between geometrically close functions, and compute the rest in the solution process. The geometry is compartmentalised into several cubes or regions that are subsequently grouped, generating higher-order regions in a hierarchical structure. Each cube at the first level includes several basis functions, and only the coupling terms with elements included in the same or neighbouring cubes are computed using the rigorous formulation and stored in the coupling matrix. The MLFMA considers the far-field interactions via efficient matrix–vector products in the iterative solution process.

The benefits of this MLFMA–MoM combination have been reported in a considerable number of publications [8, 9].

3 CBFM

In the application of the CBFM, a relatively small number of CBFs represent the unknown currents on the scenario. In a pre-processing stage, a division of the geometry into blocks is performed, each one of them supporting several CBFs. Each CBF is defined only within its associated block, whose size is generally similar or larger than a wavelength, and therefore they are also referred to as macro basis functions (MBFs). The reduced matrix computed in the CBFM is much smaller than the coupling matrix of the conventional MoM. Fig. 1*a* shows the relation between the number of unknowns of the MoM and the CBFs as the frequency increases, considering a plane plate with a side length of 1 m. As shown in Fig. 1*a*, the number of unknowns is significantly reduced for electrically larger scenarios in the CBFM.

It is possible to use different approaches for the generation of the CBFs, depending on both the accuracy and the geometrical shape of the object. It is common to use the currents induced on the surface by the plane wave spectrum (PWS) to define the CBFs. The PWS is a group of plane waves surrounding the surface and illuminating it from several directions separated by the angular steps $\Delta\theta$ and $\Delta\varphi$, and for both θ- and φ-polarisations. We have found that angular increments of $\Delta\theta = \Delta\varphi = 10°$ maintain good accuracy for 3D arbitrary cases when dealing with block sizes smaller than 4λ, while a separation of 5° between adjacent plane waves is adequate for larger blocks. After calculating the induced currents, these vectors are orthogonalised (applying, for instance the singular value decomposition, SVD) and a relatively small number of associated CBFs are retained by establishing a threshold γ with respect to the largest singular value. As a consequence, there is a reduction of the total number of CBFs by eliminating the redundancy from the original set of vectors provided.

The solution of a system of linear equations is required to determine the weights of the CBFs that represent the currents. This matrix equation reads

$$\left[\boldsymbol{Z}^R\right] \cdot \left[\boldsymbol{J}^R\right] = \left[\boldsymbol{V}^R\right] \tag{2}$$

where $[\boldsymbol{Z}^R]$ denotes the reduced matrix, containing the coupling terms between CBFs, $[\boldsymbol{J}^R]$ is the vector containing the coefficients of the current associated with each CBF and $[\boldsymbol{V}^R]$ represents the impressed voltage due to the external excitations.

4 MLFMA–CBFM

Even considering the reduced number of degrees of freedom provided by the CBFM, it is not uncommon to address problems large enough to require an exceedingly large amount of memory for the storage of the reduced matrix. This constraint can be mitigated by storing only the terms related to close blocks and considering the rest via the MLFMA using an iterative solver [8, 9, 17, 22].

There are several computational benefits derived from the use of the MLFMA–CBFM approach with respect to the conventional MoM or the previously presented MLFMA–MoM. A considerable amount of memory is dedicated to storing the aggregation and disaggregation terms and the reduced matrix. The reduction of the number of unknowns given by the CBFM results in less aggregation and disaggregation terms as well as a smaller coupling

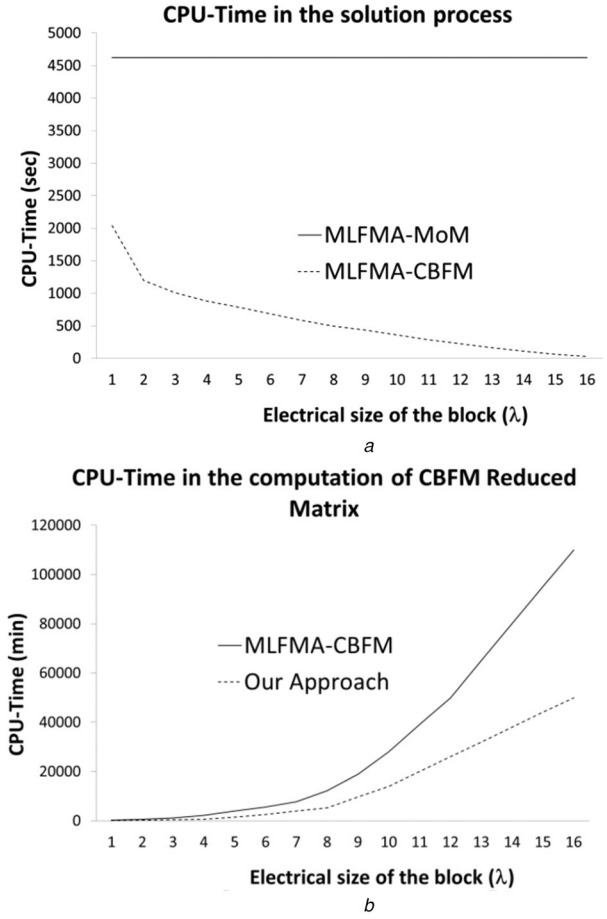

Fig. 2 *CPU-Time required*
(a) In the solution process, ***(b)*** In the calculation of the reduced matrix using the MLFMA–CBFM and the proposed technique

matrix. An additional benefit is related to the CPU time required for the analysis, due to several factors. The reduction of the number of unknowns provides a smaller equation system and decreases the time per iteration. The orthonormalisation of the CBFs generated with the SVD generally ensures an improvement of the condition number. In addition, due to the application of the MLFMA [9], the computation of the matrix–vector products required by iterative solvers is very efficient.

5 Electromagnetic kernel of the proposed technique

The reduction of the number of unknowns provided by the CBFM, as described in previous sections, improves the memory requirements and CPU time. This reduction is related to the block size, as shown in Fig. 1*b*. A 32-wavelength right-dihedron is analysed using the MoM and the CBFM for different block sizes, visualising the resulting number of unknowns. The total number of unknowns using the MoM has been 413,770.

As a consequence of the reduction of the number of unknowns, the CPU-time required by the system solution is also decreased as the block size is increased. Fig. 2*a* shows the CPU-time spent in the iterative process when analysing the dihedron test case with the MLFMA–CBFM and considering different block sizes, and compared to the MLFMA–MoM combination.

Analysing the results shown in Fig. 2*a* we can conclude that it is desirable to use large block sizes in the MLFMA–CBFM, and it results more convenient when the iterative solution process has a significant weight in the total CPU time as, for example in the analysis of ill-conditioned problems, or for monostatic RCS applications, where several excitations need to be considered. In these cases, it can be very beneficial to optimise the CPU-time per iteration, making the use of large-sized blocks highly convenient.

The drawback of using large block sizes is the increased pre-processing time required for the computation of the macro-basis functions and, especially, for the calculation of the reduced matrix $[\boldsymbol{Z}^R]$. We propose a technique for the efficient computation of the reduced matrix terms using the MLFMA, allowing to take advantage of the CPU-time reduction shown in Fig. 2*a*, while avoiding any computational burden in the calculation of the reduced matrix due to the use of large blocks.

Analysing the reduced matrix, we can note that there is a block structure in $[\boldsymbol{Z}^R]$ because each sub-matrix $[\boldsymbol{Z}^R]_{ij}$ contains the coupling terms between CBFs that are located in blocks i and j. The reduced matrix can be expressed as follows:

$$\left[\boldsymbol{Z}^R\right] = \begin{pmatrix} \left[Z^R\right]_{1,1} & \left[Z^R\right]_{1,2} & \cdots & \left[Z^R\right]_{1,K} \\ \left[Z^R\right]_{2,1} & \left[Z^R\right]_{2,2} & \cdots & \left[Z^R\right]_{2,K} \\ \vdots & \vdots & \ddots & \vdots \\ \left[Z^R\right]_{K,1} & \left[Z^R\right]_{K,2} & \cdots & \left[Z^R\right]_{K,K} \end{pmatrix} \tag{3}$$

where $[\boldsymbol{Z}^R]_{i,j}$ represents the sub-matrix embodying the coupling terms between CBFs that belong to blocks i and j. $[\boldsymbol{Z}^R]_{i,j}$ can be written as:

$$\left[\boldsymbol{Z}^R\right]_{i,j} = \begin{pmatrix} \left\langle L(J_{j,1}), W_1^i \right\rangle & \left\langle L(J_{j,2}), W_1^i \right\rangle & \cdots & \left\langle L(J_{j,Mi}), W_1^i \right\rangle \\ \left\langle L(J_{j,1}), W_2^i \right\rangle & \left\langle L(J_{j,2}), W_2^i \right\rangle & \cdots & \left\langle L(J_{j,Mi}), W_2^i \right\rangle \\ \vdots & \vdots & \ddots & \vdots \\ \left\langle L(J_{j,1}), W_{Mi}^i \right\rangle & \left\langle L(J_{j,2}), W_{Mi}^i \right\rangle & \cdots & \left\langle L(J_{j,Mi}), W_{Mi}^i \right\rangle \end{pmatrix} \tag{4}$$

where $\left\langle L(J_{j,L}), W_K^i \right\rangle$ is the inner product of the lth CBF on block j and the kth CBF on the block i. These functions are represented as aggregations of subdomain-type functions

$$J_{i,k}(u,v) = \sum_{n=1}^{N_i} \alpha_{i,k}(n) T_n(u,v) \tag{5}$$

$$W_k^i(u,v) = \sum_{n=1}^{N_i} \alpha_{i,k}(n) R_n(u,v) \tag{6}$$

where $T_n(u,v)$ and $R_n(u,v)$ denote the nth basis and testing functions on the block i. In this work, generalised rooftops and razor-blades have been selected as basis and testing functions and $\alpha_{i,k}(n)$ represents the coefficient of the CBF-k in block i, referred to as the middle point of the nth basis function. The reduced matrix elements can be computed from the low-level inner products as follows:

$$\left\langle L(J_{j,n}), W_{n'}^i \right\rangle = \sum_{k=1}^{N_{n'}} \sum_{l=1}^{N_n} \alpha_{j,n}(l) \alpha_{i,n'}^*(k) \langle T_l(u,v), R_k(u',v') \rangle \tag{7}$$

Considering the low-level MoM matrix definition for element $Z_{k,l}$, expression (15) can be written as follows:

$$\left\langle L(J_{j,n}), W_{n'}^i \right\rangle = \sum_{k=1}^{N_{n'}} \sum_{l=1}^{N_n} \alpha_{j,n}(l) \alpha_{i,n'}^*(k) Z_{k,l} \tag{8}$$

As shown in (8), in the conventional CBFM, the coupling terms of the reduced matrix associated with blocks i and j is generated using the low-level coupling terms of the conventional MoM impedance matrix belonging to the subdomains contained in the blocks in

which these CBFs are defined. If we make use of large block sizes in the CBFM, the number of low-level coupling terms can become exceedingly large, affecting the CPU time spent in the computation of the reduced matrix. In other words, the time required for the computation of the coupling term between a pair of CBFS depends on the low-level impedance matrix. Fig. 2*b* shows the CPU-time spent in the calculation of the reduced matrix with the MLFMA–CBFM and considering different block sizes.

In this work, we have made use of curved rooftops as basis functions and curved razor-blade functions as testing functions [26], but similar conclusions can be extracted for other types of low-level basis or testing functions. According to the scheme used for the definition of the low-level functions in this work, any subdomain is composed by two patches S1 and S2, and each term of the $[\boldsymbol{Z}]$ matrix, z_{ij}, is calculated as follows:

$$z_{ij} = z_{ij}^{\text{ind}} + z_{ij}^{\text{cap}} \tag{9}$$

where

$$z_{ij}^{\text{ind}} = \int_{r_a}^{r_b} \left[\frac{\text{j}\omega\mu_0}{4\pi} \int_{S_{j1}} G(\boldsymbol{r}, \boldsymbol{r}') J_j^{S_{j1}}(\boldsymbol{r}') \text{d}S' + \frac{\text{j}\omega\mu_0}{4\pi} \int_{S_{j2}} G(\boldsymbol{r}, \boldsymbol{r}') J_j^{S_{j2}}(\boldsymbol{r}') \text{d}S' \right] \text{d}l, \tag{10}$$

and

$$z_{ij}^{\text{cap}} = P^{S_{j1}}(\boldsymbol{r}_b) - P^{S_{j1}}(\boldsymbol{r}_a) - \left[P^{S_{j2}}(\boldsymbol{r}_b) - P^{S_{j2}}(\boldsymbol{r}_a) \right], \tag{11a}$$

In the previous expression, $P^{S_{j1}}(\boldsymbol{r}_b)$ is calculated from:

$$P^{S_{j1}}(\boldsymbol{r}_b) = \frac{-1}{\text{j}4\pi\omega\varepsilon_0} \int_{S_{j1}} \frac{G(\boldsymbol{r}_b, \boldsymbol{r}')}{A_{S_{j1}}} \text{d}S' \tag{11b}$$

Equations (10) and (11b) include $G(r, r')$, known as the free-space Green's function, and obtained from

$$G(\boldsymbol{r}, \boldsymbol{r}') = \frac{\text{e}^{-jk|\boldsymbol{r}-\boldsymbol{r}'|}}{|\boldsymbol{r}-\boldsymbol{r}'|} \tag{12}$$

These equations also include the $J_j^{S_{j1}}$ term, which represents the current density on patch S_{j1} belonging to subdomain-j, and $A_{S_{j1}}$ represents its area. The terms $\boldsymbol{r}'$ and $\boldsymbol{r}$ denote the position vectors for points on the patches where subdomain-j and subdomain-i are defined, respectively. Finally, and associated with subdomain-i, $\boldsymbol{r}_a$ and $\boldsymbol{r}_b$ are the end-points of its razor-blade. A more detailed description of the procedure followed to produce these expressions can be seen in [26].

In order to overcome the burden that can arise from the computation of the reduced matrix with the MLFMA–CBFM when handling large blocks, the MLFMA–MoM technique can be internally applied in order to render the reduced matrix coefficients. For this purpose, we propose the computation of the Z_{ji} term in (8), as shown in (13). This coefficient, considered for distant elements i and j and applying the electric field integral equation (EFIE), is given by the following equation:

$$z_{ji} = \int V_{mj}^{\text{AGG}_{\text{EFIE}}}(\hat{k}) \tau_{mm'}(\hat{k}, \boldsymbol{r}_{mm'}) V_{m'i}^{\text{DIS}_{\text{EFIE}}}(\hat{k}) d^2\hat{k} \tag{13}$$

where $V_{mj}^{\text{AGG}_{\text{EFIE}}}(\hat{k})$ is the aggregation term of subdomain-j to the middle point of cube-m and is computed as follows:

$$V_{mj}^{\text{AGG}_{\text{EFIE}}}(\hat{k}) = \int_u \int_v \text{e}^{-j\hat{k}\cdot\boldsymbol{r}_{jm}} (\bar{I} - \hat{k}\hat{k}) T_j(u, v) \text{d}u \, \text{d}v \tag{14}$$

where $\boldsymbol{r}_{j,m}$ is the vector that connects the integration point to the centre point of cube-m, and $T_j(u, v)$ is the basis function of the source element j.

The expression for the computation of the disaggregation term is

$$V_{m'i}^{\text{DIS}_{\text{EFIE}}}(\hat{k}) = \int_u \int_v \text{e}^{j\hat{k}\cdot\boldsymbol{r}_{jm'}} (\bar{I} - \hat{k}\hat{k}) R_i(u, v) \text{d}u \, \text{d}v \tag{15}$$

where $R_i(u, v)$ is the testing function of the destination element-i.

Analogously, for the case of the magnetic field integral equation (MFIE), we can define the coupling terms as

$$z_{ji} = \int V_{mj}^{\text{AGG}_{\text{MFIE}}}(\hat{k}) \tau_{mm'}(\hat{k}, \boldsymbol{r}_{mm'}) V_{m'i}^{\text{DIS}_{\text{MFIE}}}(\hat{k}) d^2\hat{k} \tag{16}$$

where

$$V_{mj}^{\text{AGG}_{\text{MFIE}}}(\hat{k}) = \int \int \text{e}^{-j\hat{k}\cdot\boldsymbol{r}_{jm}} T_j(u, v) \text{d}u \, \text{d}v \tag{17}$$

and

$$V_{m'i}^{\text{DIS}_{\text{MFIE}}}(\hat{k}) = -\hat{k} \times \int_u \int_v \text{e}^{j\hat{k}\cdot\boldsymbol{r}_{jm'}} R_i(u, v) \times \hat{n} \, \text{d}u \, \text{d}v \tag{18}$$

Note that $V_{mj}^{\text{AGG}}(\hat{k})$ and $V_{mj}^{\text{DIS}}(\hat{k})$ only have θ and φ components ($V_{m'i}^{\text{AGG}}(\hat{k}) = V_{\theta m'i}^{\text{AGG}}\hat{\theta} + V_{\varphi m'i}^{\text{AGG}}\hat{\varphi}$). For the computation of terms of the reduced matrix in the application of the CFIE, we combine expressions (13) and (16) weighted by the CFIE definition parameter.

Finally, the translation term between points m and m' is given by the following equation:

$$\tau_{mm'}(\hat{k}, \boldsymbol{r}_{mm'}) = \frac{jk}{4\pi} \sum_{l=0}^{L} j^l (2l+1) h_l^{(1)}(kr_{mm'}) P_l(\hat{r}_{mm'} \cdot \hat{k}) \tag{19}$$

where $P_l(x)$ is a Legendre polynomial and $h_l^{(1)}(x)$ represents the spherical Hankel function of the first kind. The integral in (13) can be truncated to a set of N_k points instead of all the directions of the unit sphere with a non-significant error. A full explanation of the appropriate number of points to be considered in this truncation is given in [9].

As mentioned earlier, the use of the MLFMA–CBFM involves the computation of the reduced matrix applying (8) for the calculation of the coupling terms between CBFs i and j, and the use of the low-level impedance matrix $\boldsymbol{Z}_{l,k}$ is required. Based on the unit theorem, we propose the use of (13) associated with the MLFMA instead of the conventional MoM coupling terms shown in (9). Therefore, the coupling term between CBFs i and j can be written (see (20)) . In order to obtain the coupling between CBFs i and j, it is possible to aggregate all the coefficients $\alpha_{i,k}(l)$ of CBF-i, associated with the low-basis function l, to the centre of its MLFMA cube m. This process can be applied for all the cubes in which CBF-i is defined. Next, the previous contributions are translated to the centre of the cubes in which CBF-j is extended and, finally, the multipole terms are disaggregated over the subdomains that define CBF-j. This procedure presents computational advantages with respect to the conventional MoM computation, although it cannot be applied for geometrically close subdomains. The existing literature recommends avoiding this algorithm for coupling terms of subdomain functions separated by a distance lower than a quarter of the wavelength [9]. The conventional MoM computation is applied for these subdomains, following (9).

For the ease of implementation, it is convenient to compartmentalise the scenario into first-level groups of a quarter of the wavelength, and then defines the CBFM block size encompassing a complete number of cubes. In order to increase the efficiency of this technique, a block size equal to a power of two

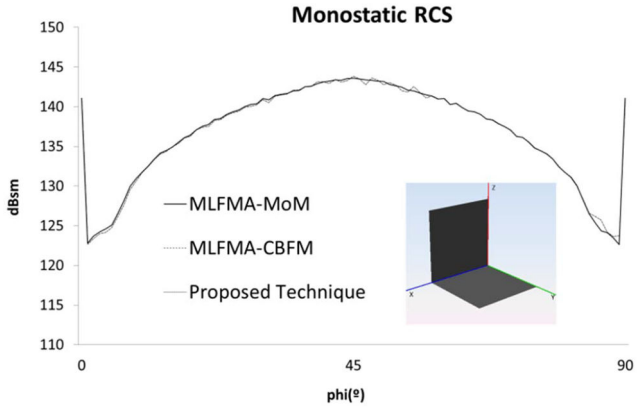

Fig. 3 *Monostatic RCS of the 32λ right-dihedron*

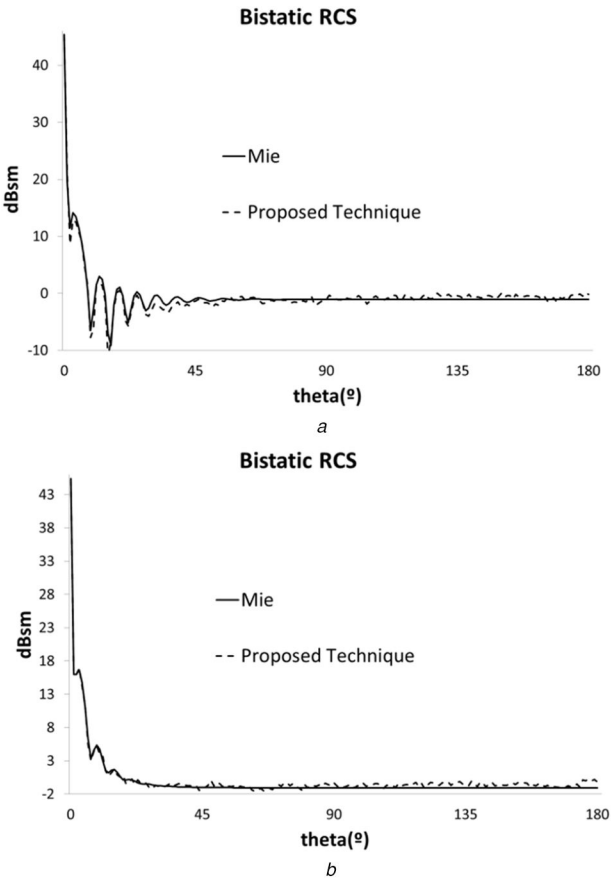

Fig. 4 *Bistatic RCS of a sphere*
(a) *H*-plane, ***(b)*** *E*-plane

with respect to the cube size is recommended, due to the nature of the MLFMA algorithm.

The main advantage of the use of the MLFMA compared to the MoM is the reduction of the complexity from N^2 to $N\log(N)$ [9], leading to a reduction of the time and memory required for the analysis. Fig. 2*b* shows the comparison of the CPU-time spent in the calculation of the reduced matrix of 32λ right-dihedron test case when applying the MLFMA–CBFM approach and the technique proposed in this paper. The CPU-time is reduced, and the ratio of the reduction is greater as the size of the block *i*ncreases, which allows the use of large blocks in order to obtain a more efficient iterative process.

As mentioned in Section 1, nowadays, the scalability and the ease in developing parallel versions of new numerical approaches play a very important role in the field. It is very valuable to obtain a technique that can be adapted to the requirements of the parallelisation paradigms for the sake of efficiency. The presented technique has a good agreement with the most popular standards of parallelisation models considering both shared and distributed memory architectures. The computer used to develop this approach contains two Intel Xeon I5 processors, each of them containing eight computation cores, and with 128 GB of RAM.

The monostatic RCS for the dihedron test case has been computed using the presented technique, and the result obtained is compared with that returned by the MoM–MLFMA and the MLFMA–CBFM techniques in Fig. 3 for the θ-polarisation and the cut φ=0° with θ ranging from 0° to 180° in steps of 1°.

As shown in Fig. 3, the proposed approach presents a good accuracy compared to the MLFMA–MoM and MLFMA–CBFM techniques. Some small differences can be appreciated between them, which can be attributed to factors such as truncation errors associated to the definition of the MLFMA (number of N_k points, numerical evaluation of the Legendre polynomial and spherical Hankel functions, etc.) as well as the generation of the CBFs (angular separation of plane waves, threshold values for the truncation of the number of CBFs, nature of the approach for the computation of the currents induced by plane waves, etc.). More details regarding these parameters are given in [9, 14].

In order to quantify the error of the proposed method, the following expression has been considered:

$$\text{Error}_{\text{approach}} = \sum_{i=1}^{N} \frac{|\text{RCS}i_{\text{MLFMA-MoM}} - \text{RCS}i_{\text{approach}}|}{|\text{RCS}_{\text{MLFMA-MoM}}|} \tag{21}$$

where N is the number of observation directions, and $\text{RCS}i_{\text{MLFMA-MoM}}$ and $\text{RCS}i_{\text{approach}}$ represent the RCS values for the *i*th direction when applying the MLFMA–MoM and the proposed approach, respectively. For this particular simulation, this error value has been 0.0326.

6 Results

First, we have considered the computation of the bistatic RCS at the frequency of 20 GHz of a sphere with a radius of 0.5 m. The analytical results are compared to those obtained with the proposed approach for the *H*- and *E*-planes, and they are shown in Fig. 4. The plane wave impinges with an angle of $\varphi = 0°$ and $\theta = 180°$ and a θ-cut at the $\varphi = 0°$ observation plane has been considered. The total number of subdomain basis functions has been 5112,144 and this number has been reduced to only 134,532 CBFs using the proposed technique. The CFIE with a residual error of 0.7×10^{-3} has been applied in order to obtain an accurate solution. The simulation has required 132 min for the reduced matrix computation and consuming 19 GB of RAM, while the MLFMA–CBFM spent about 824 min for the same analysis. This simulation has been performed using the parallelised version of the approach with 16 processors, and the block size considered has been 8λ.

The error obtained with the proposed technique using (21) has been 0.01753, considering the analytical values as the reference.

$$\begin{aligned}\left\langle L(J_{j,n}), W^i_{n'} \right\rangle &= \sum_{k=1}^{N_{n'}} \sum_{l=1}^{N_n} \alpha_{j,n}(l)\alpha^*_{i,n'}(k) Z_{k,l} \\ &= \sum_{k=1}^{N_{n'}} \sum_{l=1}^{N_n} \alpha_{j,n}(l)\alpha^*_{i,n'}(k) \int V^{\text{AGG}}_{mj}(\hat{k})\tau_{mm'}(\hat{k}, \boldsymbol{r}_{mm'}) \cdot V^{\text{DIS}}_{m'i}(\hat{k}) d^2\hat{k} \\ &= \int d^2\hat{k} \cdot \sum_{l=1}^{N_n} \alpha_{j,n}(l) V^{\text{AGG}}_{mj}(\hat{k})\tau_{mm'}(\hat{k}, \boldsymbol{r}_{mm'}) \sum_{k=1}^{N_{n'}} \alpha^*_{i,n'}(k) V^{\text{DIS}}_{m'i}(\hat{k})\end{aligned} \tag{20}$$

Table 1 Computational analysis of the sphere case

	Number of unknowns	CPU-time for pre-process, min	CPU-time for iteration, s	Memory, Gb
MLFMA–CBFM	134,532	824	57	32
proposed technique	134,532	132	57	19

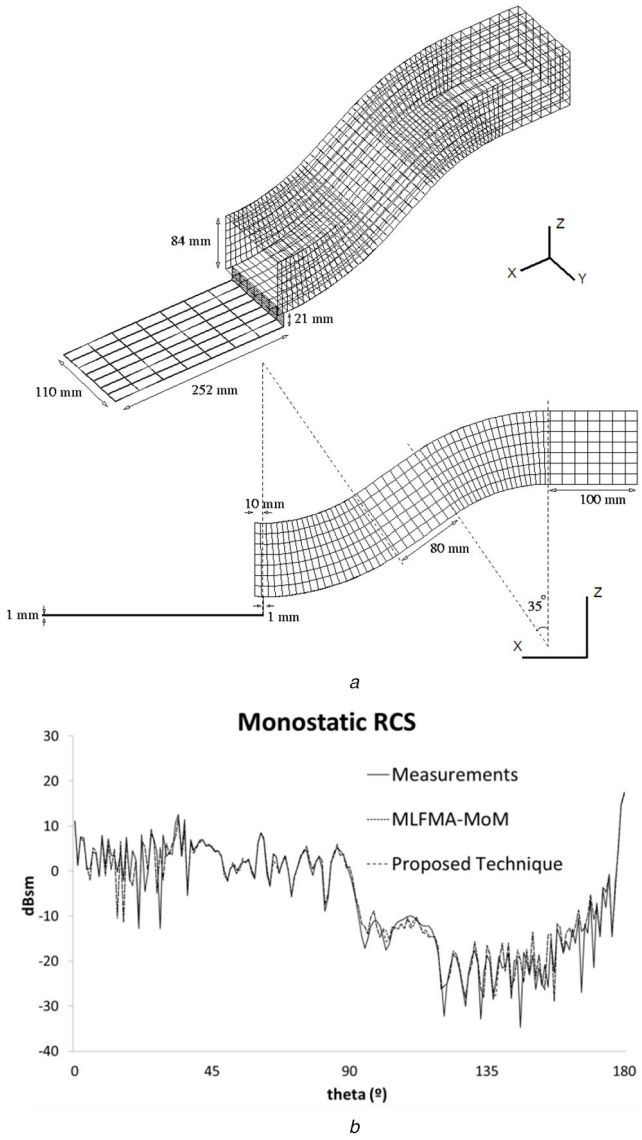

Fig. 5 *Cobra cavity test case*
(a) Geometry, ***(b)*** Monostatic RCS at 17 GHz

Table 1 shows the numerical comparison between the techniques applied for the solution of the problem.

The next test case is the computation of the monostatic RCS of the Cobra geometry, described in Fig. 5*a*, at a frequency of 17 GHz. The EFIE has been applied in the analysis, considering the θ-polarisation for the observation directions given by $\varphi = 0°$ and θ=0°–180°. The results obtained with the proposed technique have been compared to those given by the MLFMA–MoM and with measurements, as illustrated in Fig. 5*b*. Using the MLFMA–MoM, we have obtained 139,448 unknowns, while this number has been reduced to 17,632, applying the proposed technique with a block size of 8λ. The analysis has been performed using 16 processors with the parallelised version of both techniques.

A good agreement is shown between both methods and the measurements. The CPU-time and memory required for the analysis of this scenario are shown in Table 2. An error of 0.0756 has been obtained applying (21) and considering the measurement values as the reference.

Table 2 Computational analysis of the Cobra test case

	Number of unknowns	CPU-time for pre-process, min	CPU-time for iteration, s	Memory, Gb
MLFMA–MoM	139,448	183	36	6,4
MLFMA–CBFM	17,632	214	13	1,7
proposed technique	17,632	37	13	0,93

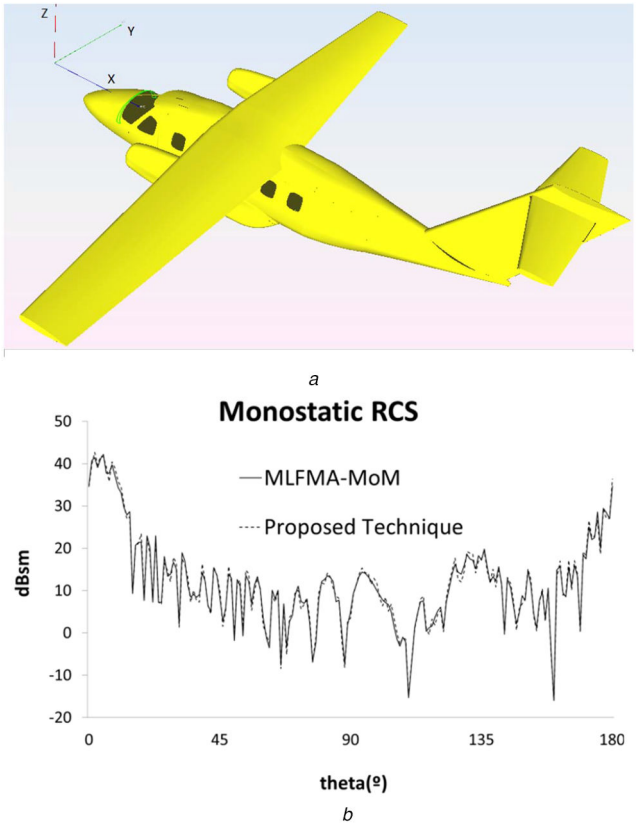

Fig. 6 *Test case at 1450 MHz*
(a) Geometry of the airplane, ***(b)*** Monostatic RCS

The next geometry considered is the airplane model shown in Fig. 6*a* considering a frequency of 1450 MHz, which has produced 694,142 unknowns when applying the MLFMA–MoM.

The monostatic RCS has been calculated applying the EFIE formulation, and the results have been compared using the MLFMA–MoM and the proposed technique. Fig. 6*b* shows the RCS for the θ-polarisation and the observation cut given by φ=180° with a variation in θ from 0° to 180° in steps of 1°. A numerical comparison between these techniques with 8 CPU-cores and a block size of 4λ is shown in Table 3. The error obtained applying (21) has been 0.06854 for this case.

Fig. 7*a* presents a new test case considering a different airplane model. The monostatic RCS has been computed at 1750 MHz. Fig. 7*b* shows the RCS results obtained for the θ-polarisation and the angular cut φ=180° where θ ranges from 0° to 180° in 1° steps. The EFIE formulation has been applied in this simulation. As in the previous cases, a good agreement is observed between the MLFMA–MoM and the proposed approach, obtaining an error of 0.05942 when applying (21).

The last test case is shown in Fig. 8*a*. This is a large object composed of 257 curved NURBS surfaces, and once again, the EFIE formulation has been applied for the analysis. The monostatic

Table 3 Computational analysis of Fig. 6*a* airplane case

	Number of unknowns	CPU-time for pre-process, min	CPU-time for iteration, s	Memory, Gb
MLFMA–MoM	694,142	268	346	63
MLFMA–CBFM	147,238	321	163	34
proposed technique	147,238	57	163	19

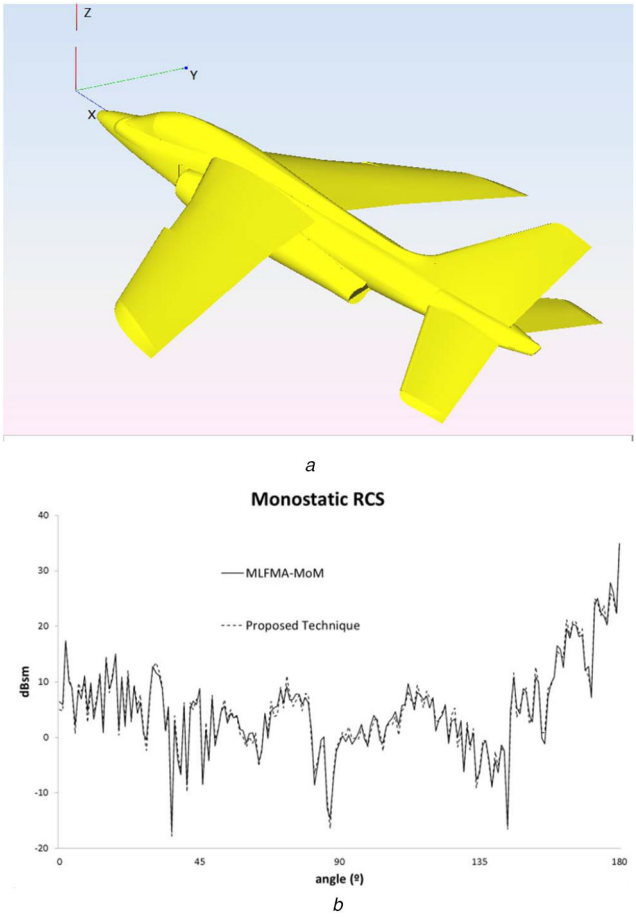

Fig. 7 *Test case at 1750 MHz*
(a) Geometry of the airplane, ***(b)*** Monostatic RCS

RCS has been computed for the θ-polarisation and for the angular observation cut given by $\varphi = 90°$ with θ between 0° and 180° in steps of 1° at a frequency of 625 MHz. The results obtained with the approach presented in this paper have been compared with MLFMA–MoM, as shown in Fig. 8*b*, where good agreement can also be observed. The error obtained in this case when applying (21) has been 0.08246.

7 Conclusions

We have proposed a method for the application of the MLFMA–CBFM approach overcoming some important limitations regarding the CPU-time required for the reduced matrix computation for large block sizes. The proposed approach has been validated in terms of accuracy while offering remarkable computational improvements derived from the increment of the block size. The conventional MLFMA–CBFM has been adapted to be able to handle large scenarios, by reducing the memory footprint and the CPU time requirements when computing the CBFM coupling matrix.

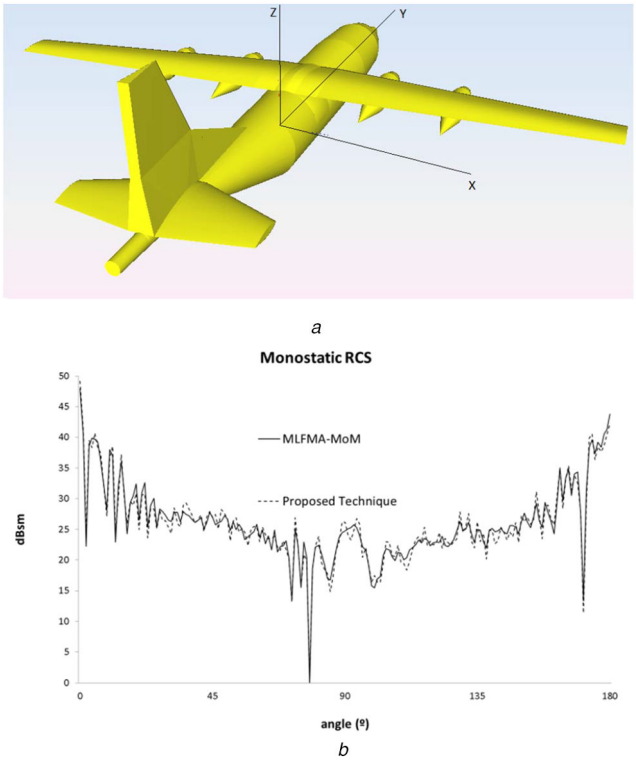

Fig. 8 *Test case at 0.625 GHz*
(a) Geometry of the airplane, ***(b)*** Monostatic RCS

8 Acknowledgments

This work was supported by the Spanish Ministry of Economy and Competitiveness Project Ref. TEC2017-89456-R, by the Junta de Comunidades de Castilla-La Mancha (Project Ref. SBPLY/17/180501/000433) and by the Universidad de Alcala projects CCG2018/EXP-048 and CCG2018/EXP-049.

9 References

[1] McNamara, D.A., Pistorius, C.W.I., Maherbe, J.A.G.: '*Introduction to the uniform geometric theory of diffraction*' (Artech House, Norwood, MA, 1990)
[2] Ruck, G.T., Barrick, D.E., Stuart, W.D., *et al.*: '*Radar cross section handbook*', vol. **1**, (Plenum Press, USA, 1970)
[3] Jakobus, U., Landstorfer, F.M.: 'Improved PO-MM hybrid formulation for scattering from three-dimensional perfectly conducting bodies of arbitrary shape', *IEEE Trans. Antennas Propag.*, 1995, **43**, pp. 162–169
[4] Thiele, G.A., Newhouse, G.A.: 'A hybrid technique for combining moment methods with the geometrical theory of diffraction', *IEEE Trans Antennas Propag.*, 1975, **23**, pp. 551–558
[5] Burnside, W.D., Yu, C.L., Marhefka, R.J.: 'A technique to combine the geometrical theory of diffraction and the moment method', *IEEE Trans. Antennas Propag.*, 1975, **AP-23**, pp. 551–558
[6] Ekelman, E.P., Thiele, G.A.: 'A hybrid technique for combining the moment method treatment of wire antennas with the GTD for curved surfaces', *IEEE Trans. Antennas Propag.*, 1980, **AP-28**, pp. 831–839
[7] Harrington, R.F.: '*Field computation by moment methods*' (McMillan, New York, 1968)
[8] Engheta, N., Murphy, W.D., Rokhlin, V., *et al.*: 'The fast multipole method (FMM) for electromagnetic scattering problems', *IEEE Trans. Antennas Propag.*, 1992, **40**, (6), pp. 634–641
[9] Chew, W.C., Jin, J., Michielssen, E., *et al.*: (Eds): '*Fast and efficient algorithms in computational electromagnetics*' (Artech House, Norwood, MA, 2001)
[10] Matekovits, L., Laza, V.A., Vecchi, G.: 'Analysis of large Complex structures with the synthetic-functions approach', *IEEE Trans. Antennas Propag.*, 2007, **55**, (9), pp. 2509–2521
[11] Suter, E., Mosig, J.R.: 'A subdomain multilevel approach for the efficient MoM analysis of large planar antennas', *Microw. Opt. Technol. Lett.*, 2000, **26**, (4), pp. 270–277
[12] Mittra, R., Du, K.: 'Characteristic basis function method for iteration-free solution of large method of moments problem', *Prog. Electromagn. Res. B*, 2008, **6**, pp. 307–336
[13] Prakash, V.V.S., Mittra, R.: 'Characteristic basis function method: a new technique for efficient solution of method of moments matrix equation', *Microw. Opt. Technol. Lett.*, 2003, **36**, (2), pp. 95–100
[14] Delgado, C., Catedra, F., Mittra, R.: 'Application of the characteristic basis function method utilizing a class of basis and testing functions defined on NURBS patches', *IEEE Trans. Antennas Propag.*, 2008, **56**, (3), pp. 784–791

[15] Saad, Y., Schultz, M.H.: 'GMRES: A generalized minimal residual algorithm for solving nonsymmetric linear systems', *SIAM J. Sci. Stat. Comput.*, 1986, **7**, (3), pp. 856–869
[16] Sleijpen, G.L.G., Fokkema, D.R.: 'Bi-CGSTAB(l) for linear equations involving unsymmetric matrices with complex spectrum', *Electron. Trans. Numer. Anal.*, 1993, **1**, pp. 11–32
[17] García, E., Moreno, J., Catedra, M.F.: 'Speeding-up the CBFM-MLFMA approach for scattering analysis of very large electromagnetic problems', *Comput. Phys. Commun.*, 2018, **232**, pp. 177–189
[18] Chen, X., Gu, C., Ding, J., *et al.*: 'Multilevel fast adaptive cross-approximation with characteristic basis functions', *IEEE Trans. Antennas Propag.*, 2015, **63**, (9), pp. 3994–4002
[19] Konno, K., Qiang, C., Sawaya, K., *et al.*: 'Optimization of block size for CBFM in MoM', *IEEE Trans. Antennas Propag.*, 2012, **60**, (10), pp. 4719–4724
[20] Gonzalez-Ovejero, D., Craeye, C.: 'Interpolatory macro basis functions analysis of non-periodic arrays', *IEEE Trans. Antennas Propag.*, 2011, **59**, (8), pp. 3117–3122
[21] Chen, X., Gu, C., Li, Z., *et al.*: 'Accelerated direct solution of electromagnetic scattering via characteristic basis function method with Sherman-Morrison-Woodbury formula-based algorithm', *IEEE Trans. Antennas Propag.*, 2016, **64**, (10), pp. 4482–4486
[22] García, E., Delgado, C., González, I., *et al.*: 'An iterative solution for electrically large problems combining the characteristic basis function method and the multilevel fast multipole algorithm', *IEEE Trans. Antennas Propag.*, 2008, **56**, (8), pp. 2363–2371
[23] Ludick, D.J., Davidson, D.B.: 'Investigating efficient parallelization techniques for the characteristic basis function method (CBFM)'. 2009 Int. Conf. on Electromagnetics in Advanced Applications (ICEAA 09), Torino, Italy, 2009
[24] García, E., Lozano, L., Algar, M.J., *et al.*: 'A study of the efficiency of the parallelization of a high frequency electromagnetic approach for the computation of radiation and scattering considering multiple bounces', *Comput. Phys. Commun.*, 2013, **184**, (1), pp. 45–50
[25] Lezar, E., Davidson, D.B.: 'GPU-Accelerated Method of moments by example: monostatic scattering', *IEEE Trans. Antennas Propag.*, 2010, **52**, (6), pp. 120–135
[26] Rivas, F., Valle, L., Cátedra, M.F.: 'A moment method formulation for the analysis of wire antennas attached to arbitrary conducting bodies defined by parametric surfaces', *Appl. Comput. Electromagn. Soc. J.*, 1996, **11**, (2), pp. 32–39